CHAPTER 6

Thorium Acylpyrazolone Complexes: Synthesis, Covalent Character, and Crystal Features.

6.1 Introduction

Research into thorium metal complexes is advancing in various fields, including nuclear energy, catalysis, and materials science [1–3]. Within the nuclear fuel cycle and weapon development, understanding the speciation of uranium and plutonium is essential for their migration pathways [4]. Uranium and thorium are particularly important within the actinide series due to their durable characteristics, studied through complex construction.

The chemistry of thorium complexes stands at the forefront of interdisciplinary research, spanning nuclear science, materials chemistry, antioxidants, and catalysis [5–8]. Thorium, a naturally occurring element with abundant reserves, holds significant promise as a versatile building block for many applications [9]. Central to these endeavours is the exploration of thorium's coordination chemistry, which underpins its behaviour in diverse chemical environments and offers avenues for tailoring its properties to specific needs [5,10]. In recent years, the chemistry of thorium complexes has garnered increasing attention due to its relevance to nuclear energy technologies [11], environmental remediation strategies [12], and catalytic processes [6]. Unlike its more widely studied counterpart, uranium, thorium exhibits distinct chemical characteristics that render it an attractive candidate for novel applications. Its propensity to form stable complexes with various ligands, coupled with its favourable nuclear properties, positions thorium as a promising element for designing advanced materials and functional molecules [5]. By unravelling the intricacies of thorium coordination chemistry, researchers are expanding our fundamental understanding of heavy element coordination and paving the way for innovative technological solutions. From the development of advanced nuclear fuels and waste management strategies to the design of catalytic systems for sustainable chemical synthesis, the chemistry of thorium complexes holds immense potential to drive scientific and technological progress in the future.

Over the past few decades, research has led to the discovery of thorium acylpyrazolone complexes, which have proven stable and offer a wide range of potential applications [13–15]. Understanding covalency in thorium metal complexes is crucial for elucidating their electronic structure and reactivity. Electronic spectra and crystallographic techniques provide insights into the degree of overlap between thorium

and ligand orbitals, the nature of metal-ligand bonding, and the coordination geometry. The original and fundamental concept of utilizing the covalent bond between metal and ligand in these complexes has been invaluable in understanding their properties.

This Chapter focuses on synthesizing thorium complexes with acyl pyrazolone ligands with the objectives mentioned above in mind. The Chapter's key points include synthesis of three Th^{4+} complexes derived from bidentate acylpyrazolone ligands, employing comprehensive characterization techniques to provide detailed bonding information and analysis and comparison of the covalent bond strengths using data obtained from characterization techniques.

6.2 Experimental section

6.2.1 Materials and Methods

HL^1, HL^2, and HL^3 ligands were synthesized and analyzed employing the methodologies outlined in our laboratory's publications [16,17]. Thorium nitrate tetrahydrate procured from SULAB Chemicals in Gujarat was introduced into the solution. The thorium concentration was determined using gravimetric techniques, expressed as ThO_2 [18]. AR-grade solvents for recrystallization were purchased from CDH Chemicals, a Central Drug House (P) Ltd division.

6.2.2 Synthesis of thorium complexes

The thorium complexes 21, 22, and 23 were synthesized using the procedure outlined in Figure 6.1 using HL^1, HL^2, and HL^3 ligands, respectively. An ethanolic ligand solution was stirred at 80-100 °C for half an hour. Subsequently, ethanolic solution of thorium nitrate was added dropwise. The solution was refluxed till precipitation.

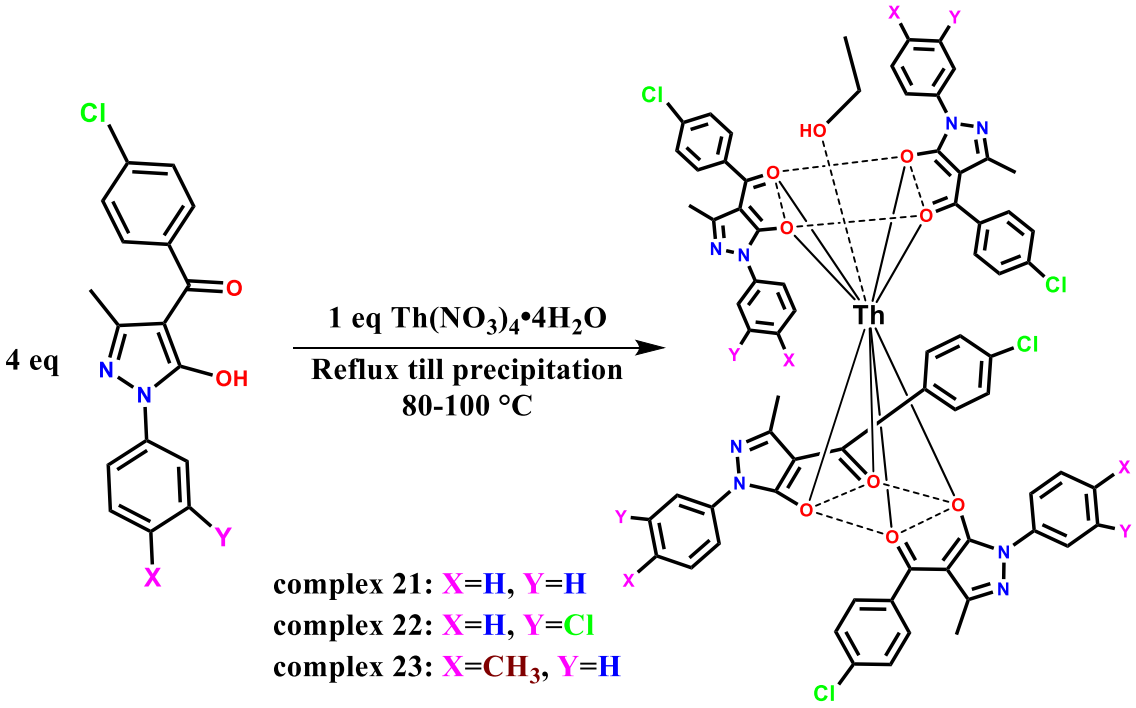

Figure 6.1 Synthetic route for thorium acylpyrazolone complexes.

Synthesis of Complex 21

Complex 21 ([Th(L^1)$_4$(EtOH)]) was prepared using HL^1 ligand (4 mmol, 1.25 g) and thorium nitrate tetrahydrate (1 mmol, 0.552 g). Yield (%): 96.34%, M.P.: > 200 °C, Molecular formula: $C_{70}H_{54}Cl_4N_8ThO_9$, Elemental analysis: C, 55.13; H, 3.57; N, 7.35%; Found: C, 55.12; H, 3.611; N, 7.50%. Formula wt: 1539.11 g mol^{-1}, % Metal (gravimetrically): Th, 14.98 %. FTIR (KBr, cm^{-1}): 1606 (C=O, p-chlorobenzoyl), 1580 (C=O, pyrazolone), 1475 (cyclic C=N). ^{1}H-NMR δ-ppm (400MHz, $CDCl_3$): 3.727 (m, 2H, $OCH_{2(CH3CH2OH)}$), 7.0-8.0 (m, Ar-H), 1.250 (t, 3H, $CH_{3(CH3CH2OH)}$).

Synthesis of Complex 22

Complex 22 ([Th(L^2)$_4$(EtOH)]) was prepared using HL^2 ligand (4 mmol, 1.39 g) and thorium nitrate tetrahydrate (1 mmol, 0.552 g). Then, it was recrystallized in DMF with a slow evaporation technique at room temperature (~32 °C), in which a DMF molecule replaced ethanol. Yield (%): 95.94%, M.P.: > 200 °C, Molecular formula: $C_{70}H_{50}Cl_8N_8ThO_9$, Elemental analysis: C, 50.56; H, 3.03; N, 6.74%; Found: C, 50.57; H, 3.037; N, 6.92%. Formula wt: 1662.86 g mol^{-1}, % Metal (gravimetrically): Th, 14.04 %. FTIR (KBr, cm^{-1}): 1602 (C=O, p-chlorobenzoyl), 1589 (C=O, pyrazolone), 1474 (cyclic C=N). ^{1}H-NMR δ-ppm (400MHz, $CDCl_3$): 3.716 (m, 2H, $OCH_{2(CH3CH2OH)}$), 7.0-8.0 (m, Ar-H), 1.242 (t, 3H, $CH_{3(CH3CH2OH)}$).

Synthesis of Complex 23

Complex 23 ([Th(L^3)$_4$(EtOH)]) was prepared using HL^3 ligand (4 mmol, 1.31 g) and thorium nitrate tetrahydrate (1 mmol, 0.552 g). Yield (%): 94.73%, M.P.: > 200 °C, Molecular formula: $C_{74}H_{62}Cl_4N_8ThO_9$, Elemental analysis: C, 56.21; H, 3.95; N, 7.09%; Found: C, 56.29; H, 3.934; N, 7.08%. Formula wt: 1581.20 g mol^{-1}, % Metal (gravimetrically): Th, 14.65 %. FTIR (KBr, cm^{-1}): 1648 (C=O, p-chlorobenzoyl), 1597 (C=O, pyrazolone), 1474 (cyclic C=N). ^{1}H-NMR δ-ppm (400MHz, $CDCl_3$): 3.727 (m, 2H, $OCH_{2(CH3CH2OH)}$), 6.8-8.0 (m, Ar-H), 1.232 (t, 3H, $CH_{3(CH3CH2OH)}$).

6.2.3 Physical measurements and characterization techniques

Analogous equipment, methods, or software was employed to analyze the statistics of synthesized compounds obtained through FTIR, TG-DTA, UV-Vis and single crystal x-ray diffraction, as previously mentioned in Chapter 3(a). Single crystal X-ray data were gathered using an XtaLAB Synergy, Dualflex, HyPix device with a graphite monochromator and Cu-K_α radiation (λ = 1.54184 Å). The diffraction data were solved, and computations were performed using the SHELXTL and SHELXL-2018/3 software packages [19,20].

6.3 Results and Discussion

The thorium acylpyrazolone complexes exhibit exceptional stability at ambient temperatures, with thorium forming covalent bonds with the ligands. Furthermore, the subsequent section elucidates the sequence of covalent bonding along with crystal formations.

6.3.1 FTIR spectral analysis

The FTIR band of υ_{O-H} indicates evidence of the binding of one CH_3CH_2OH molecule, typically observed in the 2960–3000 cm^{-1} range. This observation arises from all three complexes being synthesized using 100% ethanol as the solvent. Significant changes in the ligands' FTIR spectra upon complexation can be discerned by comparing them with their corresponding complexes [16]. As demonstrated in Table 6.1, the $\upsilon_{C=O}$ stretching frequency of the acylpyrazolone and benzoyl groups notably decreases during complexation. For instance, the $\upsilon_{C=O}$ stretching of acylpyrazolone reduces from 1590 cm^{-1} for HL^1 to 1580 cm^{-1} for complex 21, from 1590 cm^{-1} for HL^2 to 1589 cm^{-1} for complex 22, and from 1601 cm^{-1} for HL^3 to 1597 cm^{-1} for complex 23. A similar reduction is observed in the p-chlorobenzoyl carbonyl frequency (see

Table 6.1). This reduction is attributed to the shift of the O-atom charge toward the metal ions during complexation, weakening the C=O bond. Figures 6.2–6.4 depict the FTIR spectra of complexes 21–23, respectively.

Table 6.1 The FTIR values for thorium complexes (in cm^{-1}).

Code	$V_{C=O}$ benzoyl	$V_{C=O}$ acyl	Cyclic $\nu_{C=N}$	ν_{C-C} aromatic	ν_{N-N}	C-H in plane deformation
HL^1	1620	1590	1484	1357	1213	1085
Complex 21	1606	1580	1475	1378	1158	1088
HL^2	1624	1590	1484	1348	1210	1080
Complex 22	1602	1589	1474	1368	1159	1088
HL^3	1694	1601	1446	1381	1178	1071
Complex 23	1648	1597	1474	1382	1163	1088

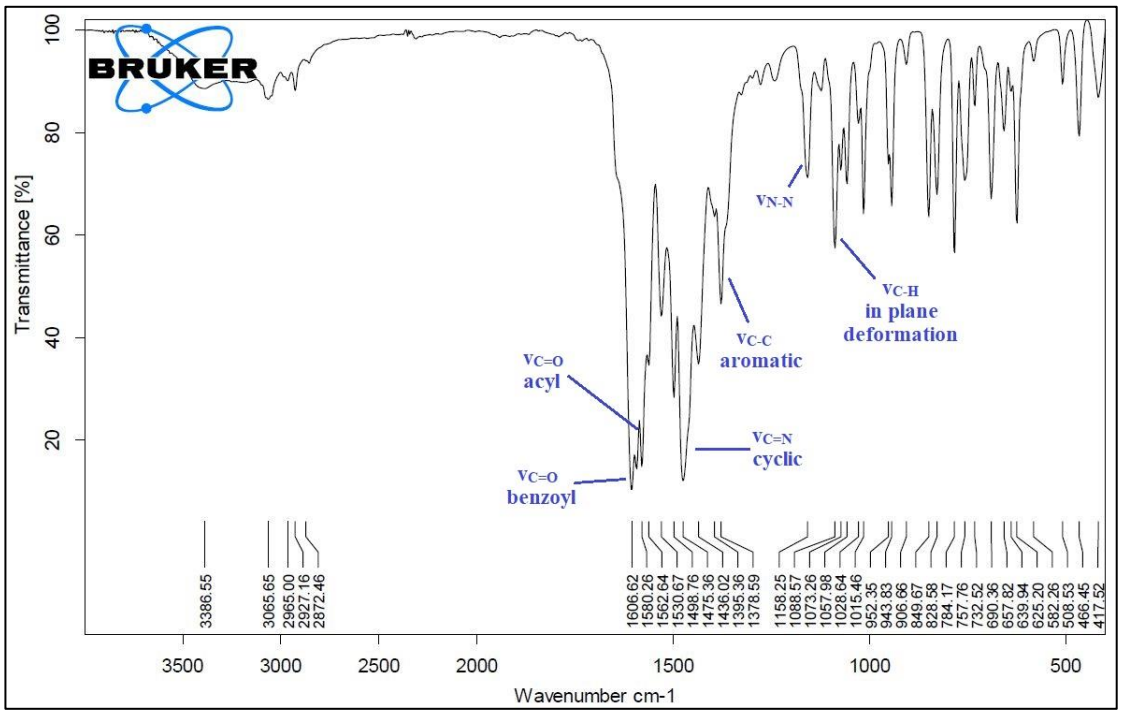

Figure 6.2 FTIR spectrum of complex 21.

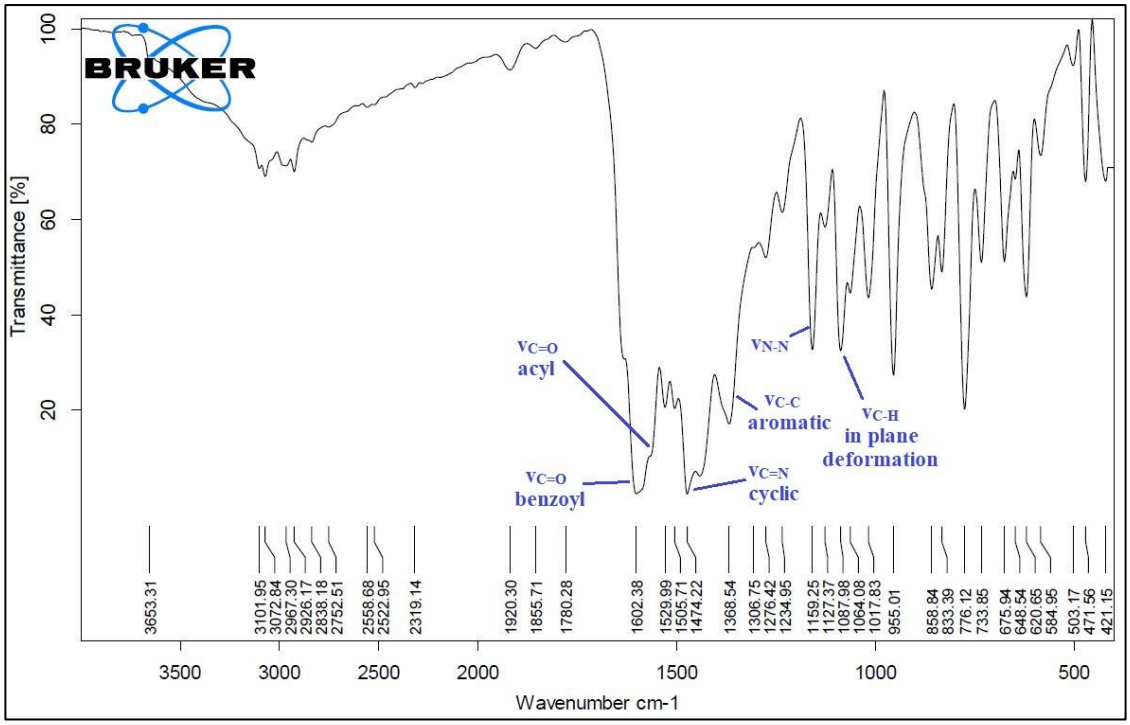

Figure 6.3 FTIR spectrum of complex 22.

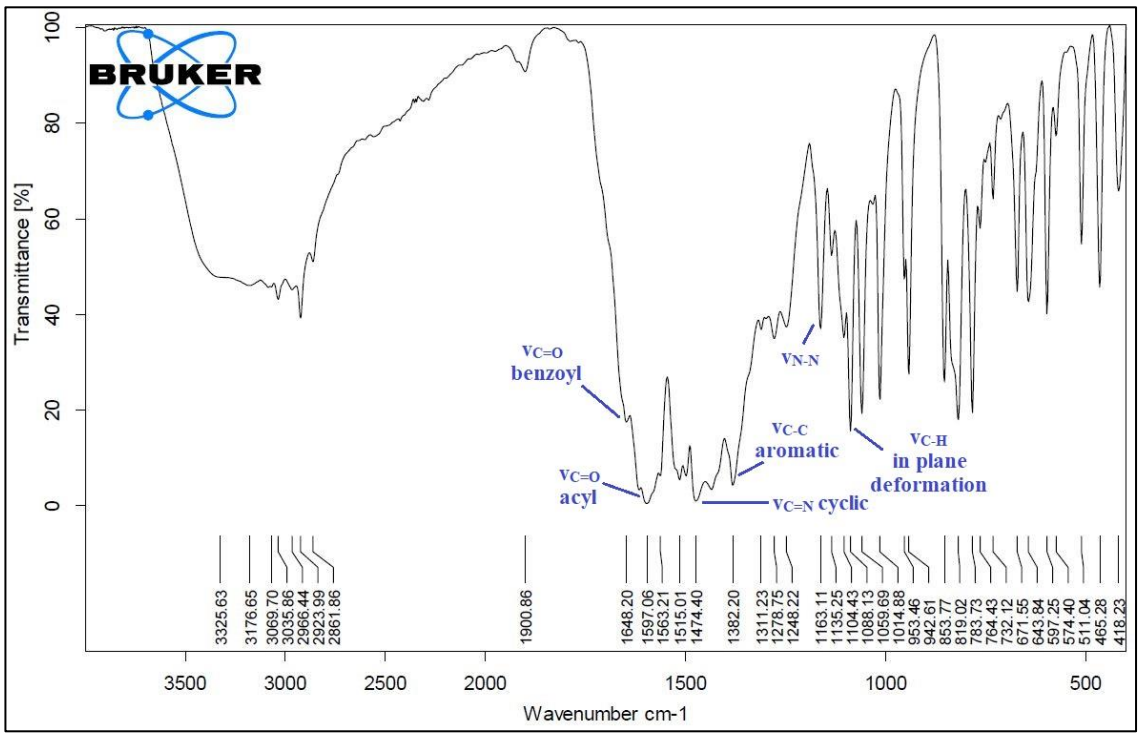

Figure 6.4 FTIR spectrum of complex 23.

6.3.2 ^{1}H-NMR spectroscopic study

The ^{1}H-NMR spectra of all representative thorium complexes were recorded in $CDCl_3$. The phenyl and methyl protons' spectra display sharp lines due to the slower relaxation time of thorium ions compared to other ions. Across all complexes, a multiplet for the OCH_2 group and a triplet for CH_3 were observed within the range of δ3.5–4.5 ppm and δ1.22–1.78 ppm, respectively. The combination of these peaks confirms the binding of an ethanolic group with the thorium ion on its ninth coordination site. The pyrazolone CH_3 appeared as many distinct lines in the complexes, displaying sharp singlets in the free ligands, indicating the arrangement of four ligands in an antisymmetric and dissimilar manner, as previously described [13,21]. An additional singlet peak of the CH_3 of p-tolyl was observed in complex 23 at δ2.287 ppm. Furthermore, multiple multiplets corresponding to aromatic protons were observed in the 6.8–8.0 ppm range in all complexes. The ^{1}H-NMR spectra of all three complexes are provided in Figures 6.5–6.7.

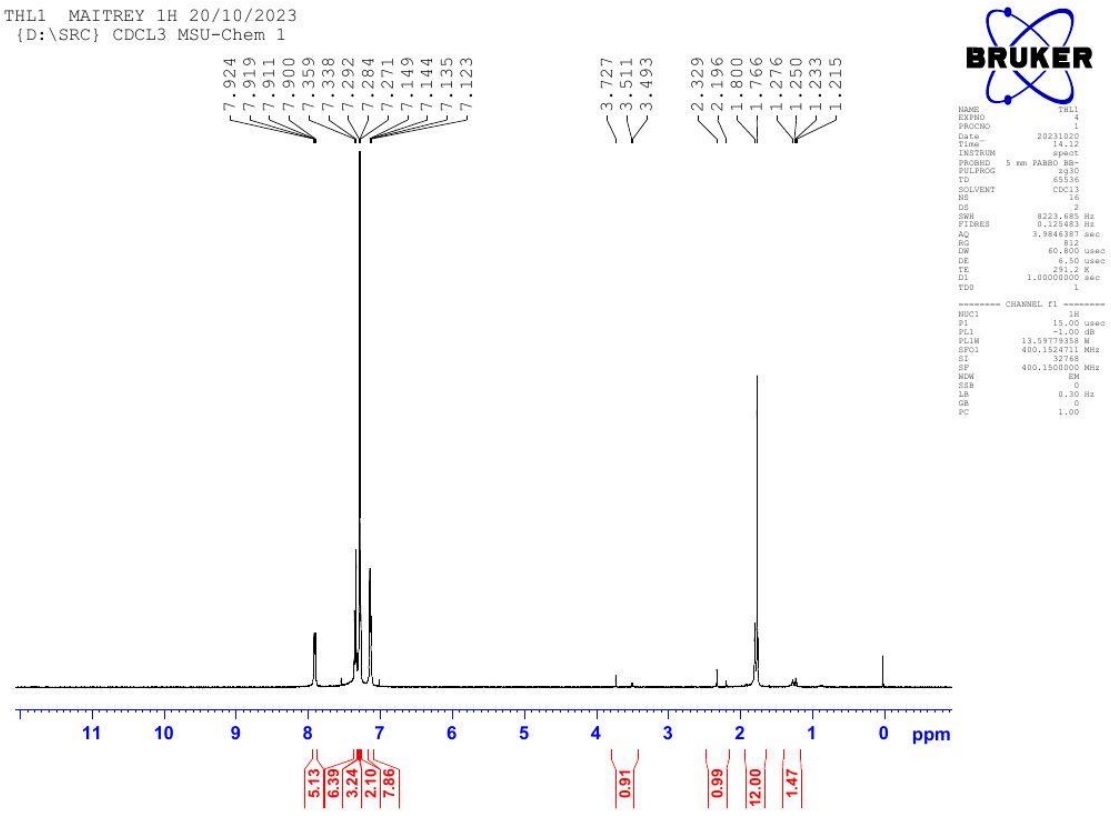

Figure 6.5 ^{1}H-NMR spectrum of complex 21.

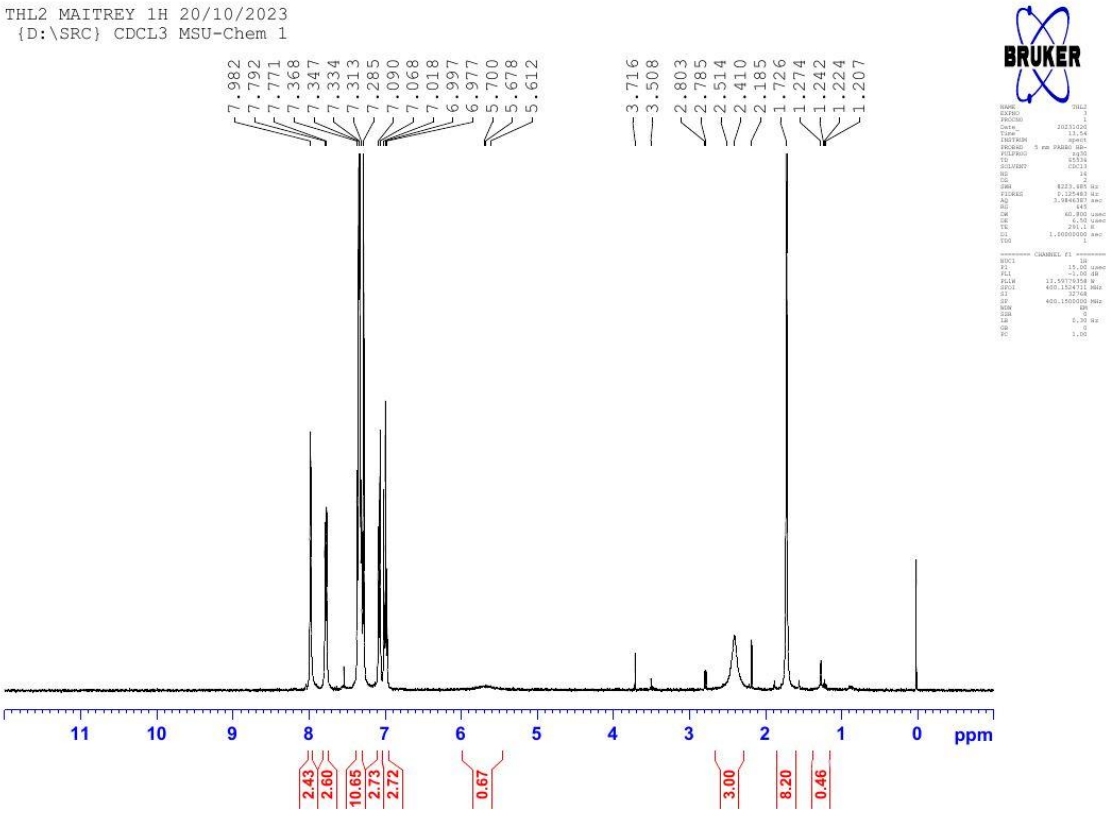

Figure 6.6 ^{1}H-NMR spectrum of complex 22.

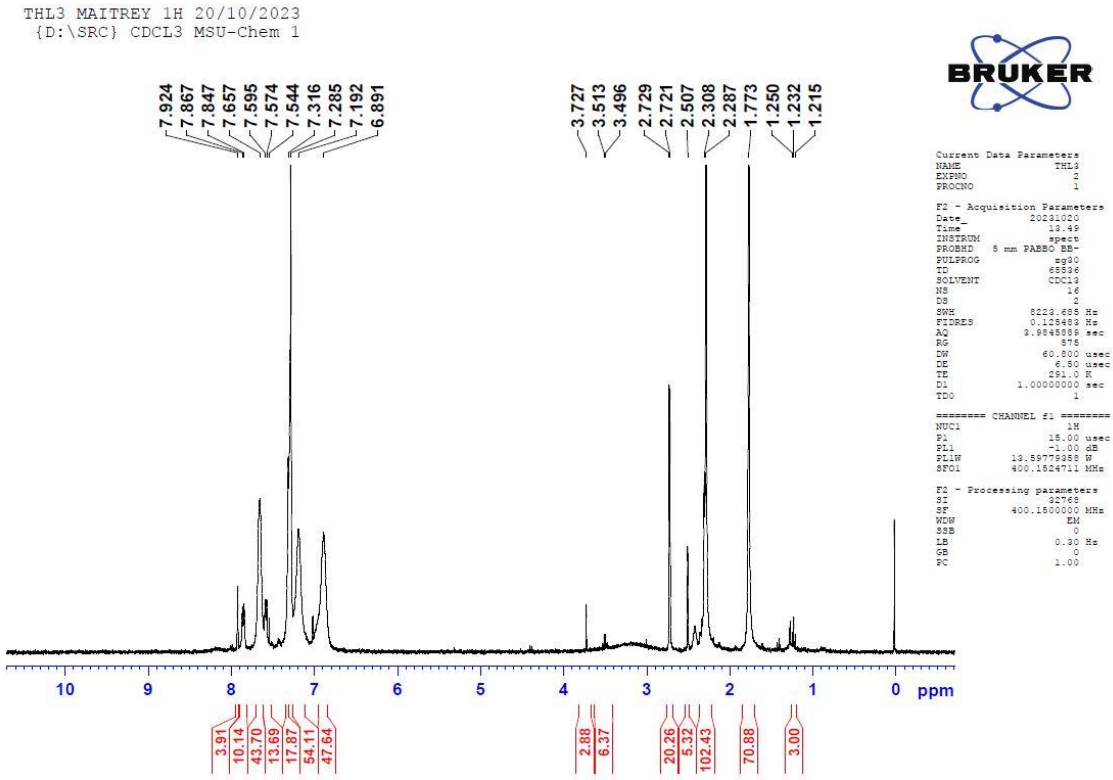

Figure 6.7 ^{1}H-NMR spectrum of complex 23.

6.3.3 Thermogravimetric analysis

Thermogravimetric analysis (TGA) data reveals a two-step breakdown process. In the first step of complex 21, the ethanol moiety is eliminated from the ninth coordination site, followed by solvent loss up to 150 °C. A significant shift of 88.3 µg/min at 100.7 °C is observed in the derivative thermogravimetric (DTG) curve. The second step involves the removal of the L^1 ligand within the temperature range of 400 to 500 °C. A sharp peak in the differential thermal analysis (DTA) curve indicates the onset of this second step, with a substantial change of 118.7 µg/min recorded at 405.3 °C (refer to the DTG curve). The final phase involves converting the metal component into thorium oxide (ThO_2). Thermogravimetric curves for all three complexes are provided in Figures 6.8–6.10. TGA curves of complexes 22 and 23 exhibit a similar pattern, with their maximum decomposition occurring during the second step in the DTG curve within the temperature range of 400–500 °C.

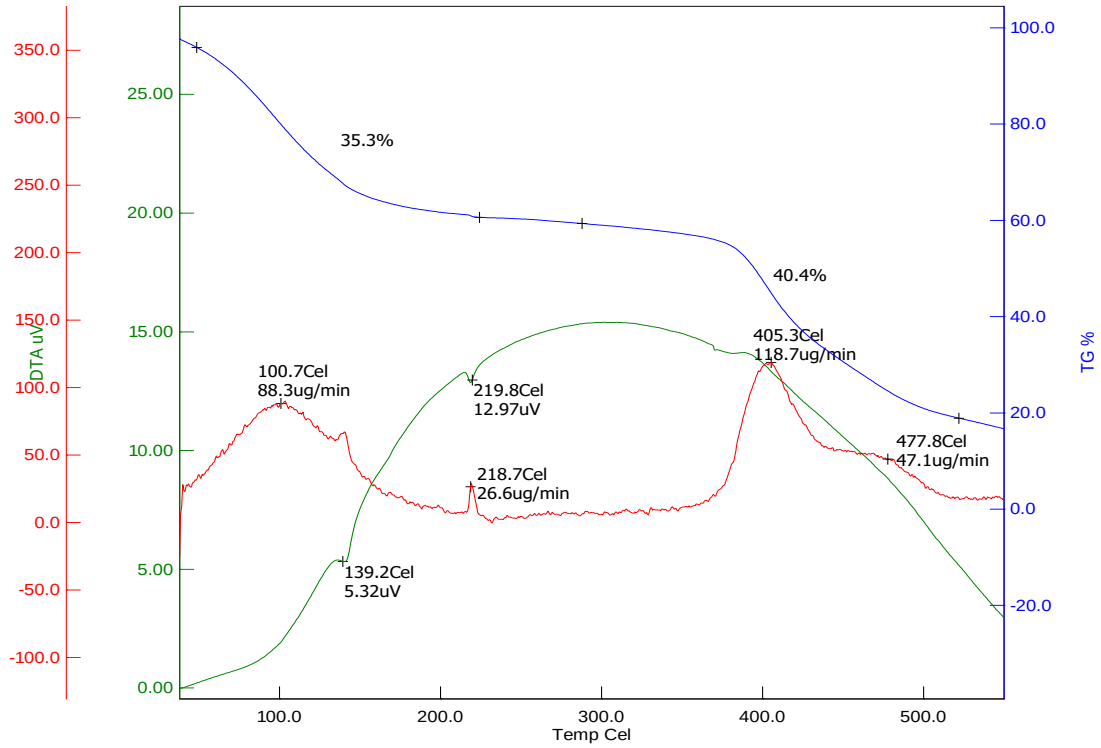

Figure 6.8 Thermogravimetric curve for complex 21.

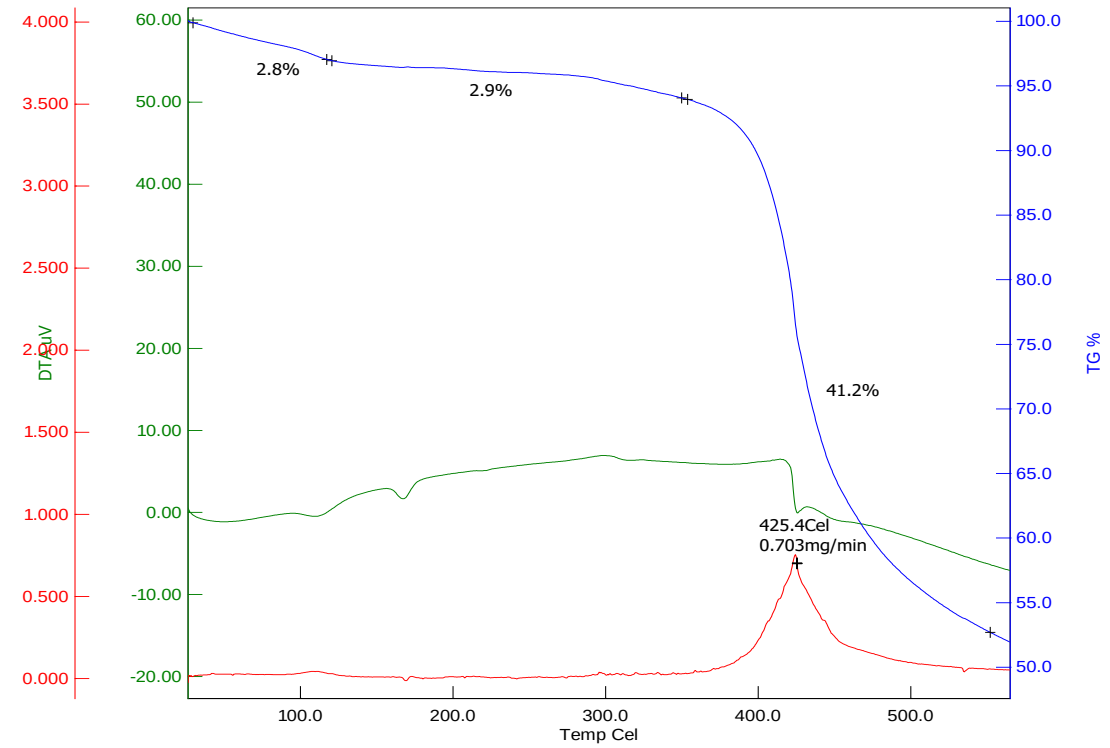

Figure 6.9 Thermogravimetric curve for complex 22.

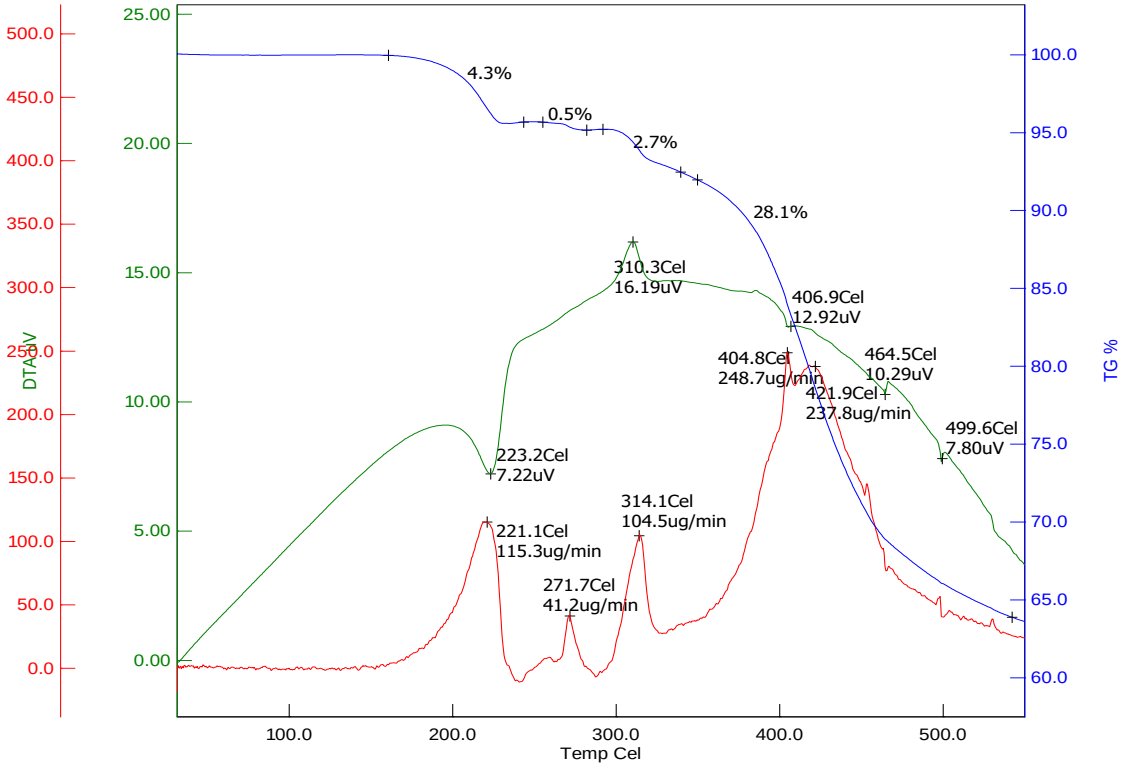

Figure 6.10 Thermogravimetric curve for complex 23.

6.3.4 Molar conductivity measurements

The molar conductivity (Λ_M) values for the ethanolic solution of complexes 21, 22, and 23 were determined to be 2.32, 2.86, and 2.50 cm^2 mol^{-1} Ω^{-1}, respectively. These relatively low values provide further evidence of non-electrolytic behaviour and the absence of charged ions within the coordination sphere [22].

6.3.5 Single crystal X-ray diffraction analysis

Bright, colourless prismatic crystals of complex 22 were obtained using a slow evaporation recrystallization technique. During recrystallization, the EtOH ligand is replaced by a DMF solvent molecule, resulting in the formation of $[Th(L^2)_2(DMF)]$ crystals. Efforts to obtain X-ray quality crystals for the other two complexes were unsuccessful, so a detailed single crystal analysis was conducted solely on the complex 22. Figure 6.11 illustrates a 2D representation of the molecular crystal structure of a colourless, prism-shaped single crystal of a thorium complex (obtained through recrystallization in DMF) with the L^2 ligand. This complex transformed the unit cell and geometry from a 12-coordination environment of thorium nitrate to a 9-coordination environment. All structural data with refinement parameters of complex 22 are provided in Table 6.2. The data of significant bond lengths and bond angles for the complex is provided in Table 6.3. Crystal of complex 22 composites through thorium bonding with four L^2 ligands in anti-manner and one DMF molecule as solvent arranged in the triclinic system with $P\ -1$ space group and monocapped square antiprismatic geometry. Figure 6.12, which displays only the pyrazolone ring atoms, illustrates the ligand arrangement in the crystal structure.

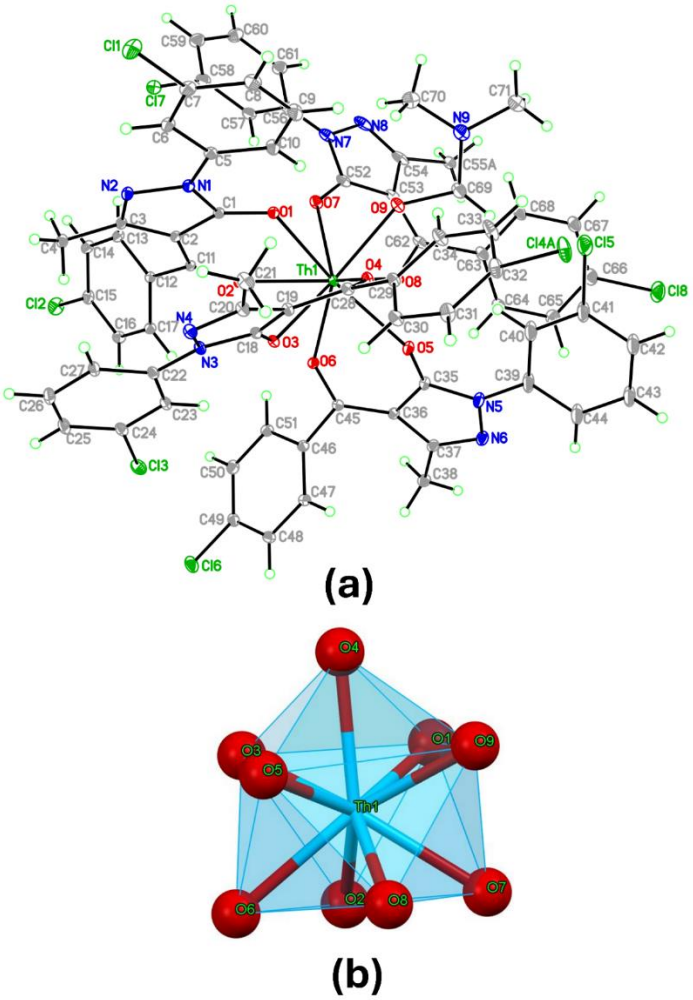

Figure 6.11 (a) Molecular structure of complex 22 with 50% ellipsoid probability, **(b)** coordination polyhedron.

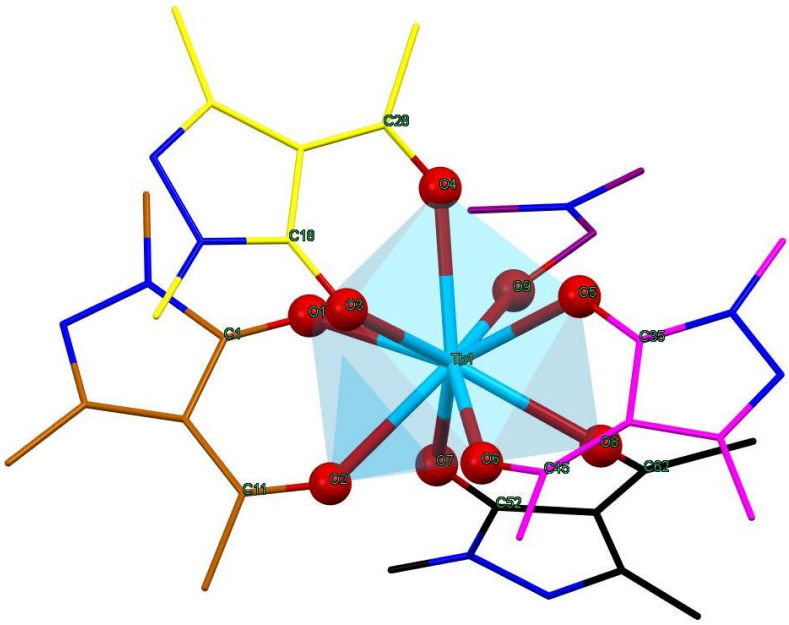

Figure 6.12 Visualization of the crystal structure of the complex 22.

Table 6.2 Crystal data and structure refinement for complex 22.

Code	Complex 22
CCDC number	2348081
Empirical formula	$C_{71}H_{51}Cl_8N_9O_9Th$
Formula weight	1689.84
Temperature	293(2) K
Wavelength	1.54184 Å
Crystal system	Triclinic
Space group	*P* −*1*
Unit cell dimensions	a = 14.72860(10) Å, α = 106.9480(10)°, b = 15.82700(10) Å, β = 94.3810(10)°, c = 17.75690(10) Å, γ = 113.4510(10)°
Volume	3544.10(5) $Å^3$
Z	2
Density (calculated)	1.584 Mg/m^3
Absorption coefficient	10.080 mm^{-1}
F(000)	1676
Crystal size	0.353 x 0.247 x 0.122 mm^3
Final R indices [I>2sigma(I)]	R_1 = 0.0343, wR_2 = 0.0923
R indices (all data)	R_1 = 0.0363, wR_2 = 0.0943
Theta range for data collection	2.666 to 76.291°
Index ranges	$-18 \le h \le 18$, $-19 \le k \le 19$, $-22 \le l \le 22$
Reflection collected	14604
Independent reflections	14604 [$R_{(int)}$ = 0.0916]
Completeness to theta = 67.679°	99.9 %
Absorption correction	Gaussian
Max. and min. transmission	0.937 and 0.076
Refinement method	Full-matrix least-squares on F^2
Goodness-of-fit on F^2	1.040
Data / restraints / parameters	14604 / 967 / 1017
Largest diff. peak and hole	1.641 and −1.281 e.$Å^{-3}$

Table 6.3 Bond parameters in complex 22.

Atoms	Bond lengths	Atoms	Bond lengths	Atoms	Bond angles	Atoms	Bond angles
Th(1)-O(9)	2.381(7)	O(3)-C(18)	1.270(4)	O(9)-Th(1)-O(5)	89.9(2)	O(9)-Th(1)-O(4)	67.2(3)
Th(1)-O(5)	2.406(3)	O(1)-C(1)	1.265(4)	O(3)-Th(1)-O(1)	75.81(9)	O(5)-Th(1)-O(4)	69.51(10)
Th(1)-O(3)	2.412(2)	O(7)-C(52)	1.281(5)	O(5)-Th(1)-O(3)	87.50(10)	O(3)-Th(1)-O(4)	68.39(8)
Th(1)-O(7)	2.425(3)	O(5)-C(35)	1.272(5)	O(9)-Th(1)-O(1)	77.4(2)	O(1)-Th(1)-O(4)	71.43(9)
Th(1)-O(6)	2.427(3)	N(1)-N(2)	1.396(4)	O(6)-Th(1)-O(2)	67.10(8)	C(1)-O(1)-Th(1)	128.5(2)
Th(1)-O(1)	2.436(2)	N(3)-N(4)	1.392(5)	O(6)-Th(1)-O(8)	74.69(10)	C(11)-O(2)-Th(1)	139.0(2)
Th(1)-O(2)	2.445(2)	N(5)-N(6)	1.407(6)	O(9)-Th(1)-O(3)	133.4(3)	C(18)-O(3)-Th(1)	127.6(2)
Th(1)-O(8)	2.462(3)	N(7)-N(8)	1.402(7)	O(5)-Th(1)-O(1)	140.85(9)	C(28)-O(4)-Th(1)	139.3(2)
Th(1)-O(4)	2.476(3)	C(36)-C(37)	1.431(6)	O(7)-Th(1)-O(6)	107.79(11)	C(35)-O(5)-Th(1)	127.6(3)
O(4)-C(28)	1.255(5)	C(2)-C(3)	1.430(5)	O(2)-Th(1)-O(8)	107.30(11)	C(45)-O(6)-Th(1)	138.2(2)
O(6)–C(45)	1.260(5)	C(19)-C(20)	1.444(5)	O(1)-C(1)-N(1)	123.5(3)	C(52)-O(7)-Th(1)	133.7(3)
O(8) –C(62)	1.262(5)	C(53)-C(54)	1.435(7)	O(1)-C(1)-C(2)	131.3(3)	C(62)-O(8)-Th(1)	135.8(3)
O(2)-C(11)	1.253(4)	O(9)-C(69)	1.491(8)	O(2)-C(11)-C(2)	122.1(3)	O(2)-C(11)-C(12)	115.2(3)

The common observation shows that the lengths of the C-O bonds in the acyl group are slightly higher than typical for C–O distance in ketones (1.23 Å) due to O→Th bonding. In comparison to Th-O(acyl) bond lengths (2.427–2.476 Å), Th-O(pyrazolone) bond lengths (2.274–2.369 Å) are slightly higher, indicating stronger covalency caused by the acyl group O-atoms. This is because longer bonds lead to a drop in the average bond order between Thorium and O-atoms, increasing covalency. Another significant observation is Th–O bond lengths. As the binding of DMF towards Th is stronger compared to L^2 ligands, the Th(1)–O(9) bond length is found to be the shortest (2.381(7) Å). Due to this effect, the Th(1)–O(4) bond becomes longer with the highest Th-O bond length (2.476 (3) Å). As provided in Figure 6.11, the upper layer of square antiprism is formed by O5, O3, O1, and O9 oxygen atoms, and similarly, the bottom layer of square antiprism is formed by O6, O2, O7, and O8 oxygen atoms. Additionally, the O4 atom remains as a cap, as observed in the polyhedral structure of complex 22 (Figure 6.11(b)). When moving from one side to another of both planes, the distance between the two planes shows a difference. This confirms that both planes are not completely parallel, and the geometry shows slight distortion (See Figure 6.13).

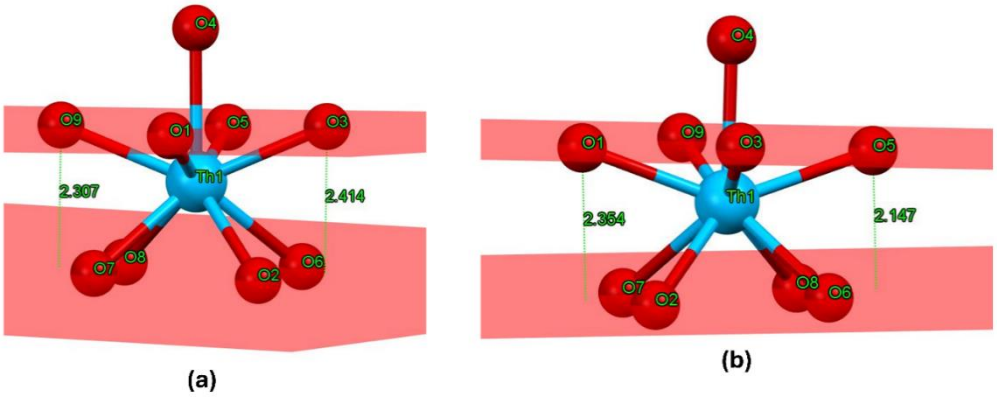

Figure 6.13 The distance between upper and bottom plane in thorium polyhedron.

6.3.6 Hirshfeld surface analysis

To visualize donor-acceptor interaction sites in complex 22, 2D FP (fingerprint) plots, mapping over d_{norm}, shape index, curvedness, fragment patch, etc., were created using Crystal Explorer 17.5 software [23]. The absence of red spots suggests a lack of hydrogen bonds in the complex. Weaker red dots are observed in d_{norm} due to more excellent proximity with closer neighbouring molecules or shorter interaction between halogen bonds as provided in Figure 6.14 [24,25]. The combination of a white-blue area also appears in d_{norm}, in which white represents the interactions equivalent to Vander-

Waals and blue represents shorter interactions than Vander-Waals interactions. A combination of red-blue curves on a curved part in the curvedness plot surrounding the aromatic rings represents shorter non-covalent interactions than Vander-Waals along with π...π stacking. It gives more stability to the crystal lattice. The shortest distances as a function of d_i and d_e from the pointed nuclei with interior and exterior to the HS respectively provided a piece of surface points and combined give d_{norm} area. Curvedness is a function of the rms (root mean square) curvature of the HS, in which a flat surface and sharp surface represent low and high curvedness, respectively. As provided in shape index diagrams, the concave surface on oxygen atoms of ligands has appeared as a dark yellow-orange shade with less than zero shape index value, which gives evidence of metal-ligand interactions in the complex. The colour patches on the HS depend on their closeness to adjacent molecules. Percentage data for atom-all and all-atom interactions provide an idea about the packing probability in complex crystal (See Figure 6.15). Two-dimensional fingerprint plots equivalent to all these interactions are provided in Figure 6.16.

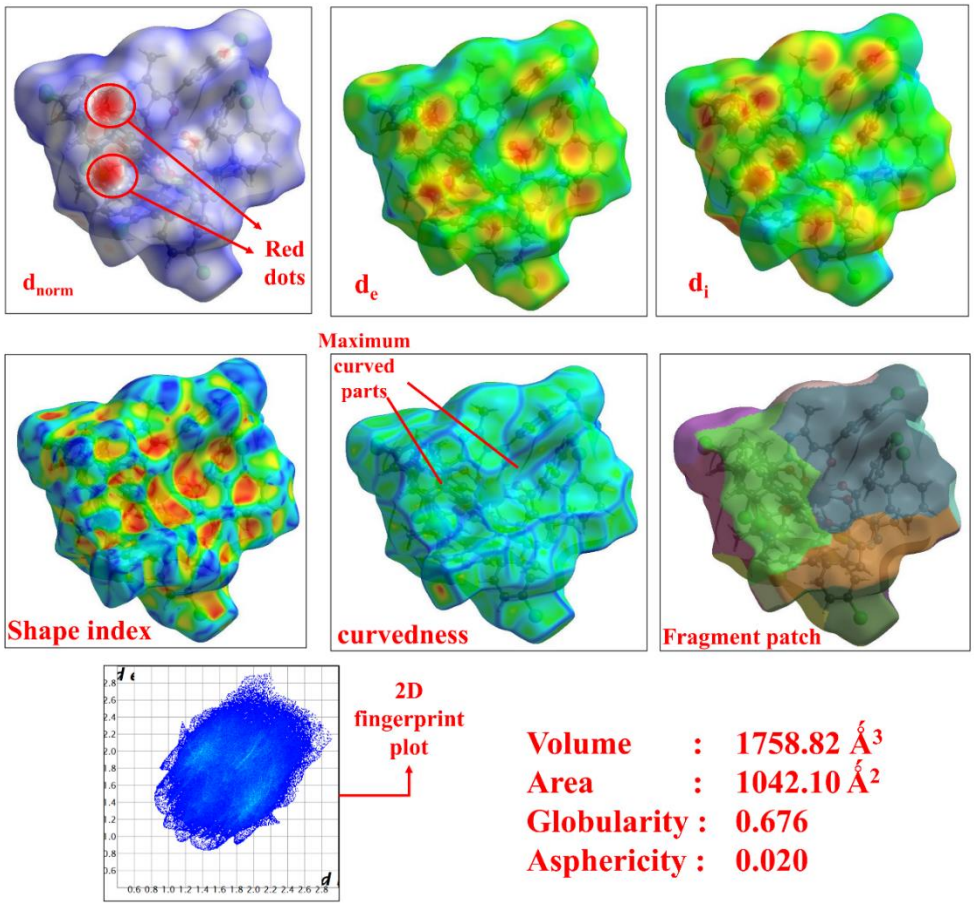

Figure 6.14 Molecular Hirshfeld surfaces in complex 22.

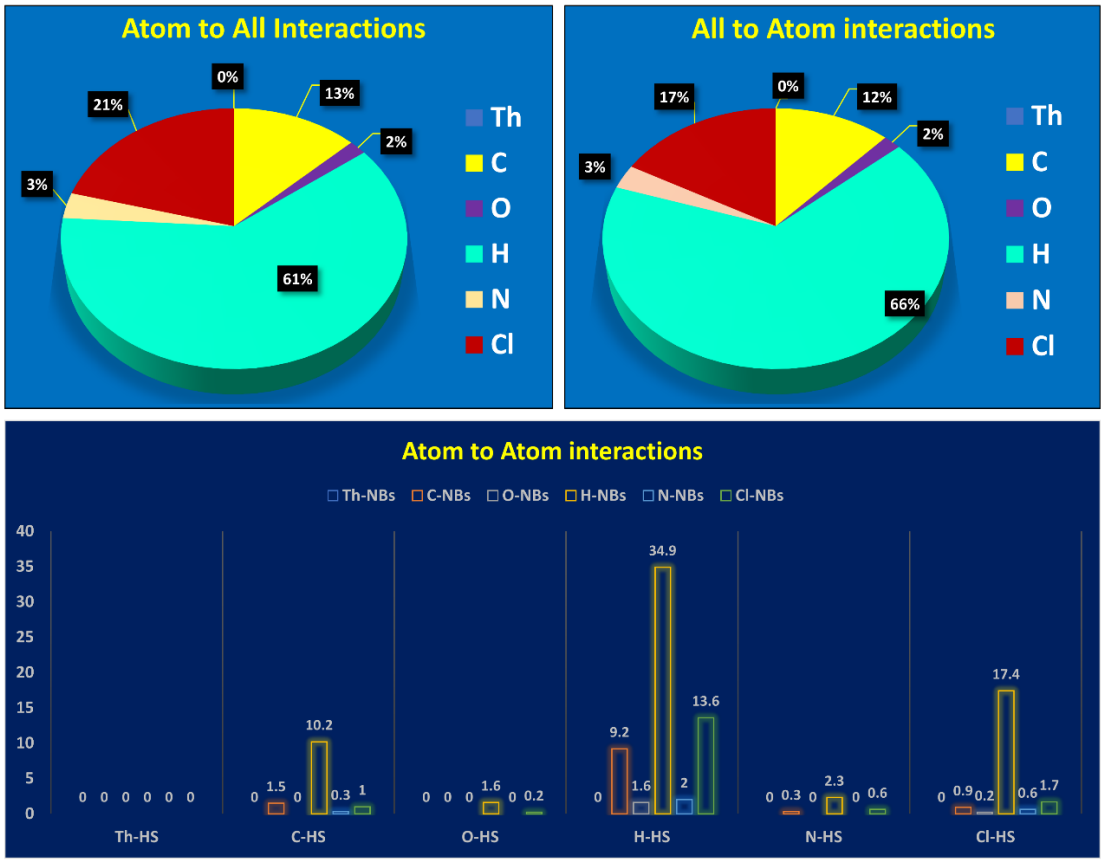

Figure 6.15 Graphical presentation of percentage interactions in complex 22.

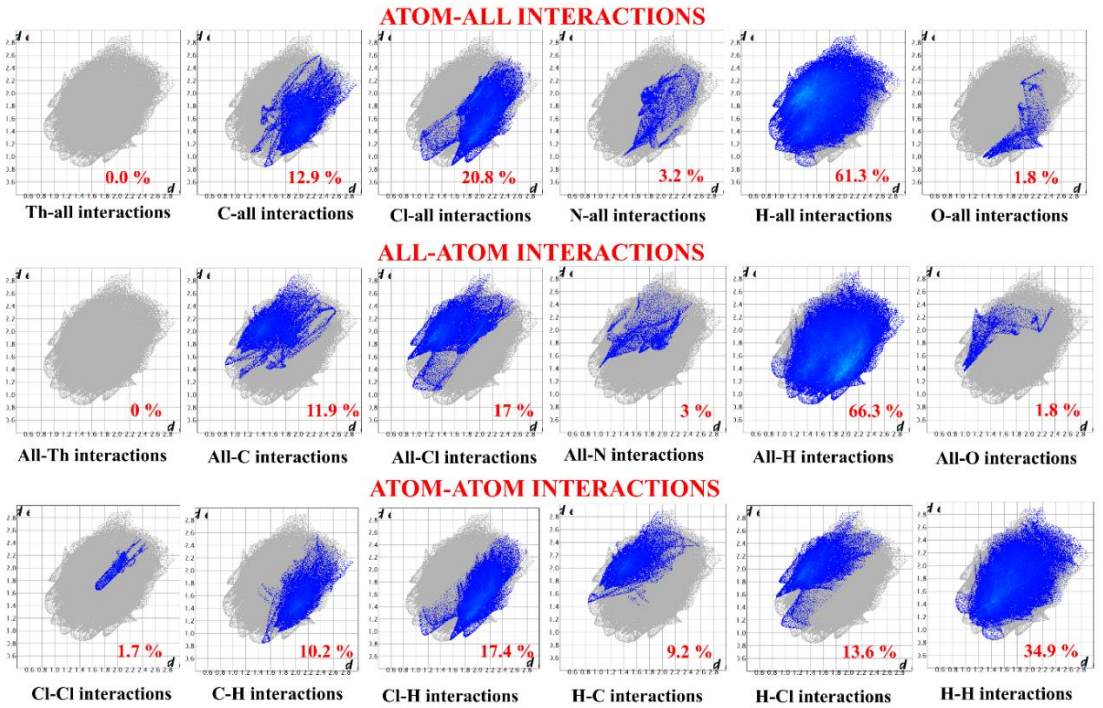

Figure 6.16 Two-dimensional fingerprint plots in complex 22.

6.3.7 Electronic spectral analysis

The UV-Vis electronic spectral studies were carried out for complexes 21, 22, and 23 in 10^{-6} M solutions of $CHCl_3$, DMF, and DMSO solvent, and the spectra are provided in Figure 6.17. Since thorium is in a +4 oxidation state, only n→π*, π→π*, and LMCT transitions appeared for complexes in the 200−500 nm range, respectively. To demonstrate the covalency of complexes 21, 22, and 23, covalency parameters were used to compute the Nephelauxetic ratio (β), Sinha parameter (δ%), bonding parameter ($b^{1/2}$), and angular overlap parameter (η) [26–29]. In Nephelauxetic ratio calculation, $\bar{\nu}_{complex}$ and $\bar{\nu}_{free\ ion}$ (41394 cm^{-1}) were identified by taking peak centre values for all transitions in the absorption spectra of complexes. All covalency parameters were calculated using the following equations.

$$\text{Nephelauxetic ratio } \boldsymbol{\beta} = \frac{\bar{\nu}_{complex}}{\bar{\nu}_{free\ ion}} \quad (6)$$

$$\text{Sinha parameter } \boldsymbol{\delta}\% = \left[\frac{1-\beta}{\beta}\right] \times 100 \quad (7)$$

$$\text{Bonding parameter } b^{\frac{1}{2}} = \left(\frac{1-\beta}{2}\right)^{1/2} \quad (8)$$

$$\text{Angular overlap parameter } \eta = \frac{1-\sqrt{\beta}}{\sqrt{\beta}} \quad (9)$$

Table 6.4 Calculated values of covalency parameters for complexes 21, 22, and 23.

Complex	Solvent	Peak center value (in cm^{-1})	Nephelauxetic ratio B	Bonding parameter $b^{\frac{1}{2}}$	Sinha parameter δ	Angular overlap parameter η
21	$CHCl_3$	39370	0.9511	0.1564	5.141	0.0254
	DMF	34005	0.8215	0.2988	21.7292	0.1033
	DMSO	34341	0.8296	0.2919	20.5381	0.0979
22	$CHCl_3$	39472	0.9536	0.1524	4.8693	0.0241
	DMF	34025	0.822	0.2983	21.6576	0.103
	DMSO	34321	0.8291	0.2923	20.6084	0.0982
23	$CHCl_3$	39356	0.9508	0.1569	5.1784	0.0256
	DMF	34530	0.8342	0.2879	19.8784	0.0949
	DMSO	34344	0.8297	0.2918	20.5276	0.0979

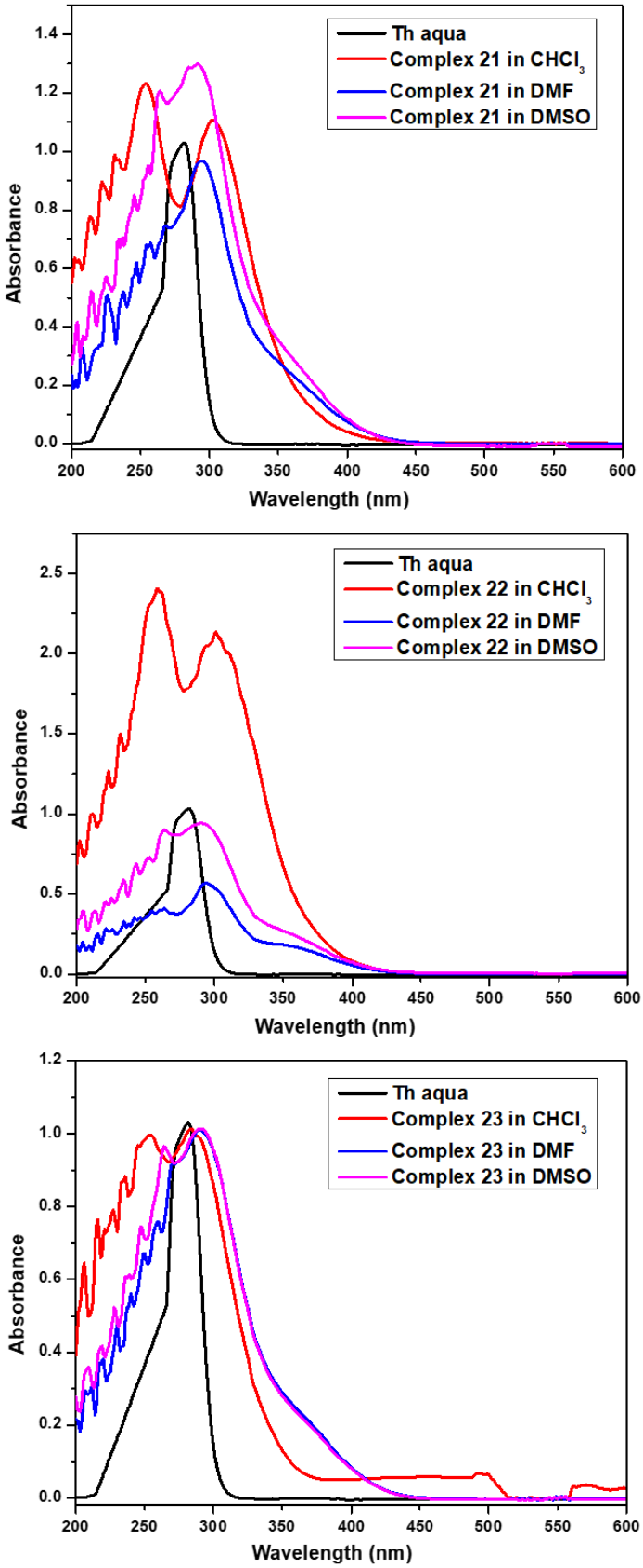

Figure 6.17 Electronic UV-Vis spectra for complexes 21, 22, and 23 in 10^{-6} M solutions of $CHCl_3$, DMF, and DMSO solvents.

The thorium acylpyrazolone series is best understood through the data mentioned above, and by comprehending the covalent character of these complexes, various chemical properties and applications can be explored. Positive bonding parameter values and minimal changes suggest covalent bonding with limited 5f-orbital participation in the synthesized complexes across all solvents, where the nephelauxetic effect ranges from 0.8215 to 0.9536. The Sinha parameter (δ%) and angular overlap parameter (η), both indicating electron delocalization across the 5f orbital and covalency, are positive for all complexes, signifying a degree of covalent bonding in $Th^{(IV)}$ complexes. The degree of covalent character typically follows the order DMF > DMSO > $CHCl_3$, as indicated by the Sinha parameter values in Table 3. The slight variation in the bonding parameter value suggests relatively less involvement of 5f-orbitals in the bonding of thorium-acylpyrazolone complexes [25].

6.4 Conclusions

Three monocapped square antiprismatic thorium complexes were synthesized using bidentate acylpyrazolone ligands. Their characterization has been done using all available techniques, such as IR, NMR, single-crystal X-ray diffraction, TG-DTA, UV-VIS, etc. These characterized data are largely used to examine their structure, geometry, composition, surface interactions, and covalent character. Electronic spectral studies were carried out to calculate Covalency parameters (Nephelauxetic ratio, Sinha parameter, Bonding parameter, Angular Overlap Parameter) to get covalency order in different solvents. Calculating the covalency parameters demonstrates the electron delocalization across the 5f orbital and the covalency, both positive for all complexes, suggesting an analogous degree of covalent bonding. The thorium acylpyrazolone series can be best understood using the data mentioned above, and by understanding the covalent character of these complexes in order, it is possible to investigate various chemical properties and applications.

References

[1] R.J.M. Konings, O. Beneš, J.-C. Griveau, 2.01 - The Actinides Elements: Properties and Characteristics, in: R.J.M. Konings (Ed.), Comprehensive Nuclear Materials, Elsevier, Oxford, 2 (2012) 1–20. https://doi.org/10.1016/B978-0-08-056033-5.00008-2.

[2] E. Capelli, R.J.M. Konings, 7.07 - Halides of the Actinides and Fission Products Relevant for Molten Salt Reactors, in: R.J.M. Konings, R.E. Stoller (Eds.), Comprehensive Nuclear Materials (Second Edition), Elsevier, Oxford, 7 (2020) 256–283. https://doi.org/10.1016/B978-0-12-803581-8.11794-1.

[3] R.C. Ewing, Safe management of actinides in the nuclear fuel cycle: Role of mineralogy, Comptes Rendus. Géoscience 343 (2011) 219–229. https://doi.org/10.1016/j.crte.2010.09.003.

[4] A.Yu. Romanchuk, I.E. Vlasova, S.N. Kalmykov, Speciation of Uranium and Plutonium From Nuclear Legacy Sites to the Environment: A Mini Review, Front Chem 8 (2020). https://www.frontiersin.org/articles/10.3389/fchem.2020.00630.

[5] C.D. Tutson, A.E. V Gorden, Thorium coordination: A comprehensive review based on coordination number, Coord Chem Rev 333 (2017) 27–43. https://doi.org/10.1016/j.ccr.2016.11.006.

[6] J. Leduc, M. Frank, L. Jürgensen, D. Graf, A. Raauf, S. Mathur, Chemistry of Actinide Centers in Heterogeneous Catalytic Transformations of Small Molecules, ACS Catal 9 (2019) 4719–4741. https://doi.org/10.1021/acscatal.8b04924.

[7] F. Ortu, A. Formanuik, J.R. Innes, D.P. Mills, New vistas in the molecular chemistry of thorium: low oxidation state complexes, Dalton Trans 45 (2016) 7537–7549. https://doi.org/10.1039/C6DT01111J.

[8] A. Pushpaveni, S. Packiaraj, S. Poornima, L. Kousalya, S. Govindarajan, Structural and multi-functional properties of novel thorium complex bearing higher analogue of guanidine base, Mater Chem Phys 275 (2022) 125213. https://doi.org/10.1016/j.matchemphys.2021.125213.

[9] Z.-J. Li, X. Guo, J. Qiu, H. Lu, J.-Q. Wang, J. Lin, Recent advances in the applications of thorium-based metal–organic frameworks and molecular clusters, Dalton Trans 51 (2022) 7376–7389. https://doi.org/10.1039/D2DT00265E.

[10] T. Ünak, What is the potential use of thorium in the future energy production technology?, Progress in Nuclear Energy 37 (2000) 137–144. https://doi.org/10.1016/S0149-1970(00)00038-X.

[11] P. Soudek, A. Hrdinová, I.M. Rodriguez Valseca, Z. Lhotáková, M. Mihaljevič, Š. Petrová, M. Kofroňová, K. Moťková, J. Albrechtová, T. Vaněk, Thorium as an environment stressor for growth of Nicotiana glutinosa plants, Environ Exp Bot 164 (2019) 84–100. https://doi.org/10.1016/j.envexpbot.2019.03.027.

[12] F. Marchetti, C. Pettinari, R. Pettinari, Acylpyrazolone ligands: Synthesis, structures, metal coordination chemistry and applications, Coord Chem Rev 249 (2005) 2909–2945. https://doi.org/10.1016/j.ccr.2005.03.013.

[13] F. Marchetti, R. Pettinari, C. Pettinari, Recent advances in acylpyrazolone metal complexes and their potential applications, Coord Chem Rev 303 (2015) 1–31. https://doi.org/10.1016/j.ccr.2015.05.003.

[14] F. Marchetti, C. Pettinari, C. Di Nicola, A. Tombesi, R. Pettinari, Coordination chemistry of pyrazolone-based ligands and applications of their metal complexes, Coord Chem Rev 401 (2019) 213069. https://doi.org/10.1016/j.ccr.2019.213069.

[15] I. Shaikh, R.N. Jadeja, R. Patel, Three mixed ligand mononuclear Zn(II) complexes of 4-acyl pyrazolones: Synthesis, characterization, crystal study and anti-malarial activity, Polyhedron 183 (2020) 114528. https://doi.org/10.1016/j.poly.2020.114528.

[16] I. Shaikh, R.N. Jadeja, R. Patel, V. Mevada, V.K. Gupta, 4-Acylhydrazone-5-Pyrazolones and their Zinc(II) Metal Complexes: Synthesis, Characterization, Crystal Feature and Antimalarial Activity, J Mol Struct 1232 (2021) 130051. https://doi.org/10.1016/j.molstruc.2021.130051.

[17] A.I. Vogel, Vogel's textbook of quantitative chemical analysis, Fifth edition. Harlow, Essex, England: Longman Scientific & Technical; New York: Wiley (1989). https://search.library.wisc.edu/catalog/999612906602121.

[18] G.M. Sheldrick, Crystal structure refinement with SHELXL, Acta Crystallogr Section C 71 (2015) 3–8. https://doi.org/10.1107/S2053229614024218.

[19] G.M. Sheldrick, SHELXT – Integrated space-group and crystal-structure determination, Acta Acta Crystallogr Section A 71 (2015) 3–8. https://doi.org/10.1107/S2053273314026370.

[20] M.S. Nagar, P.B. Ruikar, M.S. Subramanian, Complexes of tetravalent plutonium, uranium and thorium with acylpyrazolones, Inorganica Chim Acta 141 (1988) 309–312. https://doi.org/10.1016/S0020-1693(00)83925-0.

[21] W.J. Geary, The use of conductivity measurements in organic solvents for the characterization of coordination compounds, Coord Chem Rev 7 (1971) 81–122. https://doi.org/10.1016/S0010-8545(00)80009-0.

[22] P.R. Spackman, M.J. Turner, J.J. McKinnon, S.K. Wolff, D.J. Grimwood, D. Jayatilaka, M.A. Spackman, CrystalExplorer: a program for Hirshfeld surface analysis, visualization and quantitative analysis of molecular crystals, J Appl Crystallogr 54 (2021) 1006–1011. https://doi.org/10.1107/S1600576721002910.

[23] A.P. Novikov, M.A. Volkov, A.V. Safonov, M.S. Grigoriev, Synthesis, Crystal Structure, and Hirshfeld Surface Analysis of Hexachloroplatinate and Tetraclorouranylate of 3-Carboxypyridinium—Halogen Bonds and π-Interactions vs. Hydrogen Bonds, Crystals (Basel) 12 (2022) 271. https://doi.org/10.3390/cryst12020271.

[24] M.K. Patel, U.H. Patel, S.A. Gandhi, V.M. Barot, J. Jayswal, Solvent effect on neutral Co (II) complexes of paeonol derivative –qualitative and quantitative studies from energy framework and Hirshfeld surface analysis, J Mol Struct 1196 (2019) 119–131. https://doi.org/10.1016/j.molstruc.2019.06.050.

[25] H. Debecca Devi, Ch. Sumitra, Th. David Singh, N. Yaiphaba, N. Mohondas Singh, N. Rajmuhon Singh, Calculation and Comparison of Energy Interaction and Intensity Parameters for the Interaction of Nd(III) with DL-Valine, DL-Alanine and β-Alanine in Presence and Absence of Ca^{2+}/Zn^{2+} in Aqueous and Different Aquated Organic Solvents Using 4f-4f Transition Spectra as Probe, Int J Spectrosc 2009 (2009) 1–9. https://doi.org/10.1155/2009/784305.

[26] M.C. Chavan, P. V Vaidya, N.R. Lokhande, M.N. Ghoshal, Bonding and Energy Parameters for Some Praseodymium(III) Mixed Ligand Complexes, Indian J Chem Sect A: Inorg Phys Theor Anal 23 (2010) 530–532. http://inis.iaea.org/search/search.aspx?orig_q=RN:18050308.

[27] S.P. Sinha, Spectroscopic investigations of some neodymium complexes, Spectrochim Acta 22 (1966) 57–62. https://doi.org/10.1016/0371-1951(66)80008-5.

[28] K. Iftikhar, Hypersensitivity in the 4f–4f absorption spectra of lanthanide(III) complexes, Inorganica Chim Acta 129 (1987) 261–264. https://doi.org/10.1016/S0020-1693(00)86672-4.

Published Papers:

Journal of Molecular Structure 1318 (2024) 139295

Contents lists available at ScienceDirect

Journal of Molecular Structure

journal homepage: www.elsevier.com/locate/molstr

Covalency parameters for nine-coordinated thorium acylpyrazolone complexes along with their synthesis and crystal features

Maitrey Travadi [a], Dr Rajendrasinh N. Jadeja [a,*], Ray J. Butcher [b]

[a] Department of Chemistry, Faculty of Science, The Maharaja Sayajirao University of Baroda, Vadodara 390002, India
[b] Department of Inorganic & Structural Chemistry, Howard University, Washington, DC, 22031, USA

ARTICLE INFO

Keywords:
Monocapped square antiprismatic thorium
acylpyrazolone complex
Single crystal
Covalency parameter

ABSTRACT

This study discusses the synthesis and characterization of three thorium complexes with a general composition of $[Th(L)_4(EtOH)]$ demonstrated a nine-coordinated geometry in acylpyrazolone chemistry, a novel finding supported by single crystal evidence. A detailed analysis of complex $[Th(L^2)_2(DMF)]$ was conducted, utilizing single-crystal X-ray diffraction data and Hirshfeld surface area analysis to investigate secondary interactions, exploring the planarity and bonding characteristics of the crystals. Covalency parameters such as the Nephelauxetic ratio, Sinha parameter, bonding parameter, and angular overlap parameter were calculated from electronic spectral data, revealing positive covalency and electron delocalization across the 5f orbital for all complexes. Notably, the presence of solvent bound to the 9th coordination site of the complex suggests potential changes in covalency across different solvents, thereby indirectly impacting chemical characteristics.

1. Introduction

Research into thorium metal complexes is advancing in several fields including nuclear energy, catalysis, and materials science [1–3]. Within the nuclear fuel cycle and weapon development, understanding the speciation of plutonium and uranium is essential for their resettling pathways [4]. The chemistry of thorium complexes stands at the forefront of interdisciplinary research, spanning the fields of nuclear science, materials chemistry, antioxidant, and catalysis [5–8]. Thorium, a naturally occurring element with abundant reserves, holds significant promise as a versatile building block for a myriad of applications [9]. Central to these endeavours is the exploration of thorium's coordination chemistry, which underpins its behaviour in diverse chemical environments and offers avenues for tailoring its properties to specific needs [5, 10]. In recent years, the chemistry of thorium complexes has garnered increasing attention due to its relevance to nuclear energy technologies [11], environmental remediation strategies [12], and catalytic processes [6]. Unlike its more widely studied counterpart, uranium, thorium exhibits distinct chemical characteristics that render it an attractive candidate for novel applications. Its propensity to form stable complexes with a variety of ligands, coupled with its favourable nuclear properties, positions thorium as a promising element for the design of advanced materials and functional molecules [5]. By unravelling the intricacies of thorium coordination chemistry, researchers are not only expanding our fundamental understanding of heavy element coordination but also paving the way for innovative technological solutions. From the development of advanced nuclear fuels and waste management strategies to the design of catalytic systems for sustainable chemical synthesis, the chemistry of thorium complexes holds immense potential to drive scientific and technological progress in the years to come.

Generally, thorium(IV)-imido complexes exhibit a higher basic character and lower covalent character compared to cerium(IV)-imido complexes [13]. Kelsen and their research group have examined the covalent properties of the Zr-O bond in zirconium complexes with both fluorinated and nonfluorinated hydroxyborate salts, utilizing their single crystal data [14]. DFT calculations reported by Liu et al. indicated that 2-phosphaethynolate complexes follow a covalency trend of U–O > Th–O > Ti–O, attributed to the involvement of 5f orbitals [15]. Research by Kloditz and colleagues indicates that the study of chemical bonding in $[M(salen)_2]$ type complexes focuses on the degree of covalency in the bonds to various donor atoms and the relative involvement of 5f and 6d orbitals [16]. Kaltsoyannis reported studies on $AnCp_4$ and $AnCp_3$ complexes, showing that as the actinide series progresses, the metal-carbon bond exhibits increased covalency (based on orbital mixing and spin densities) [17]. In 2021, Sittel et al. reported on the influence of solvent polarity on the ligand configuration in tetravalent thorium N-donor

* Corresponding author.
E-mail address: rjadeja-chem@msubaroda.ac.in (D.R.N. Jadeja).

https://doi.org/10.1016/j.molstruc.2024.139295
Received 16 May 2024; Received in revised form 6 July 2024; Accepted 12 July 2024
Available online 14 July 2024